

Absorption Linear Dichroism Measured Directly on a Single Light-Harvesting System: The Role of Disorder in Chlorosomes of Green Photosynthetic Bacteria

Shu Furumaki,[†] Frantisek Vacha,[‡] Satoshi Habuchi,[†] Yusuke Tsukatani,[§] Donald A. Bryant,[§] and Martin Vacha^{*,†}

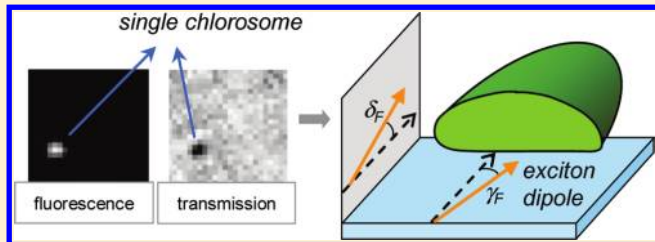
[†]Department of Organic and Polymeric Materials, Tokyo Institute of Technology, Ookayama 2-12-1-S8, Meguro-ku, Tokyo 152-8552, Japan

[‡]Institute of Physical Biology, University of South Bohemia and Institute of Plant Molecular Biology, Academy of Sciences of the Czech Republic, Branišovská 31, České Budějovice 370 05, Czech Republic

[§]Department of Biochemistry and Molecular Biology, The Pennsylvania State University, University Park, Pennsylvania 16802, United States

 Supporting Information

ABSTRACT: Chlorosomes are light-harvesting antennae of photosynthetic bacteria containing large numbers of self-aggregated bacteriochlorophyll (BChl) molecules. They have developed unique photophysical properties that enable them to absorb light and transfer the excitation energy with very high efficiency. However, the molecular-level organization, that produces the photophysical properties of BChl molecules in the aggregates, is still not fully understood. One of the reasons is heterogeneity in the chlorosome structure which gives rise to a hierarchy of structural and energy disorder. In this report, we for the first time directly measure absorption linear dichroism (LD) on individual, isolated chlorosomes. Together with fluorescence-detected three-dimensional LD, these experiments reveal a large amount of disorder on the single-chlorosome level in the form of distributions of LD observables in chlorosomes from wild-type bacterium *Chlorobaculum tepidum*. Fluorescence spectral parameters, such as peak wavelength and bandwidth, are measures of the aggregate excitonic properties. These parameters obtained on individual chlorosomes are uncorrelated with the observed LD distributions and indicate that the observed disorder is due to inner structural disorder along the chlorosome long axis. The excitonic disorder that is also present is not manifested in the LD distributions. Limiting values of the LD parameter distributions, which are relatively free of the effect of structural disorder, define a range of angles at which the excitonic dipole moment is oriented with respect to the surface of the two-dimensional aggregate of BChl molecules. Experiments on chlorosomes of a triple mutant of *Chlorobaculum tepidum* show that the mutant chlorosomes have significantly less inner structural disorder and higher symmetry, compatible with a model of well-ordered concentric cylinders. Different values of the transition dipole moment orientations are consistent with a different molecular level organization of BChl's in the mutant and wild-type chlorosomes.



1. INTRODUCTION

Chlorosomes are large light-harvesting antenna structures found in green sulfur bacteria or green filamentous bacteria,^{1,2} and recently also in *Acidobacteria*.³ They have ovoid shapes with dimensions $\sim 150 \text{ nm} \times 60 \text{ nm} \times 30 \text{ nm}$, and contain $\sim 200,000$ bacteriochlorophyll (BChl) *c*, *d*, or *e* molecules.^{1,4} Molecules of BChl self-assemble without any protein scaffolding into large aggregates,⁵ which, together with carotenoids and quinones, form the cores of chlorosomes. The aggregation leads to unique photophysical properties: chlorosomes are able to capture the incident light and transfer it to reaction centers with high efficiency. These features enable bacteria with chlorosomes to survive phototrophically at very low light intensities^{6,7} and make chlorosomes ideal models for organic photovoltaic devices, artificial photosynthesis or molecular electronics.

There has been a continued interest in the structure behind the unique functional properties of chlorosomes.⁸ However, because of their inherent compositional and morphological heterogeneity, the structural arrangement of the BChl's in chlorosomes cannot be determined by crystallographic methods, and different structural models of long-range order, such as quasi-one-dimensional (1D) rods^{9,10} or two-dimensional (2D) lamellae¹¹ have been proposed on the basis of electron microscopy (EM) and X-ray measurements.^{9–13} A recent cryo-EM study of chlorosomal cross sections¹⁴ revealed that BChl's self-assemble into large 2D-aggregate sheets that form higher-order structures of various shapes, such as concentric cylinders, scrolls, or curved lamellae.

Received: December 21, 2010

Published: April 08, 2011

In the case of a well-ordered triple mutant of *Chlorobaculum tepidum* (formerly known as *Chlorobium tepidum*) as well as the wild-type strain, it was shown that the aggregates comprise *syn*–*anti* monomer stacks and that the sheets are rolled up to form mainly complete, enclosed concentric cylinders.¹⁵

Even though the mesoscopic, long-range chlorosome structure is accessible by the above methods, there is still a lack of consensus about the molecular-level or short-range order of the BChl's in the 2D-aggregates, which has mainly been studied by NMR and other techniques.^{15–19} As demonstrated by the close correspondence of Fourier transforms of structural models and cryo-EM images of BChl's at high resolution,¹⁵ the chlorosomes of *C. tepidum* are an exception. The molecular-level structure is responsible for the excitonic properties of chlorosomes and should conform to the observed absorption, linear and circular dichroic spectra. The difficulty in determining the molecular-level structure and excitonic properties stems from the compositional heterogeneity and the resulting hierarchy of structural disorder present in chlorosomes. The structural heterogeneity is manifested, e.g., as inhomogeneous broadening and splitting of proton signals in ¹³C-enriched chlorosomes in solid state NMR.²⁰ The different levels of disorder include:

1. Ensemble disorder, that is, even within the same species and under the same cultivation conditions there are differences between individual chlorosomes.¹⁴
2. Mesoscopic inner structural disorder, that is, within one chlorosome there are domains of varying sizes in which the 2D-aggregates can be arranged differently in the x – y -plane and which are oriented slightly differently with respect to the long (z) axis (refer to Figure 1a for the definition of the coordinate system).
3. Excitonic (intradomain) disorder which originates from disorder of the molecular-level ordering. This type of disorder can be diagonal (due to dispersion of transition frequencies of individual BChl's) or off-diagonal (due to dispersion in the coupling strength between individual BChl's).

All three types of disorder usually contribute to the observed spectral properties in ensemble optical experiments. The use of single-molecule detection and spectroscopy removes the highest level of disorder. Further, correlation between different observables helps to associate the remaining types of disorder. Single-molecule spectroscopy has previously been applied to the study of chlorosomes and provided information on their fluorescence spectral and polarization anisotropy.²¹

Here, we describe the direct detection of absorption by individual photosynthetic light-harvesting complexes for the first time. We measure absorption linear dichroism (LD) on individual wild-type (WT) chlorosomes from the green sulfur bacterium *C. tepidum* and correlate the observed data with three-dimensional (3D) LD detected via fluorescence. We obtain large distributions of the LD parameters due to the inherent structural disorder and relate them with fluorescence spectra measured on the same individual chlorosomes. Analysis of the LD distributions provides a range of possible orientations of the exciton transition dipole moment angle with respect to the surface of the 2D-aggregates and also provides information about the symmetry of the distribution of the dipoles. The results were then compared to absorption LD measured on individual chlorosomes from a well-ordered *bchQ bchR bchU* triple mutant of *C. tepidum*.²² As expected from the recently determined structure,¹⁵

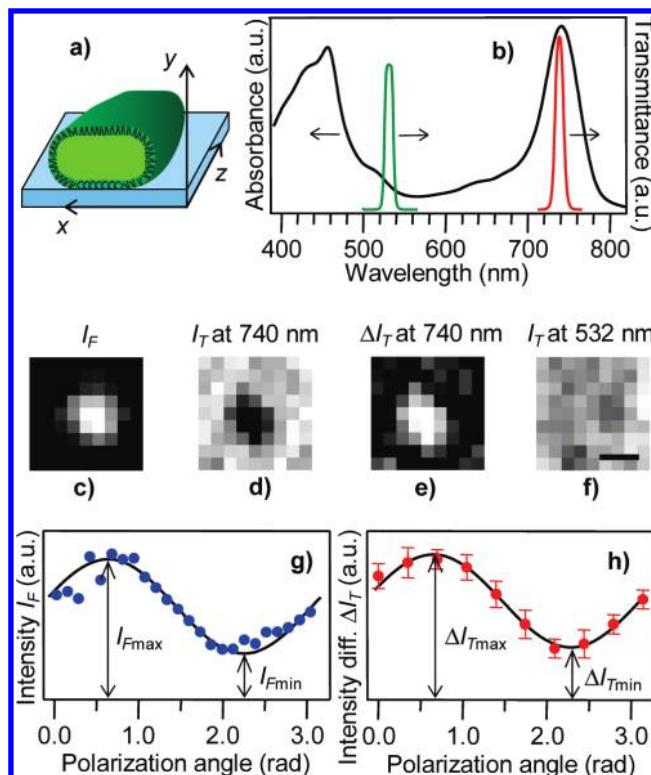


Figure 1. Principle of the single-chlorosome absorption detection method. (a) Schematic depiction of the chlorosome and its orientation on the substrate. (b) Absorption spectrum of WT chlorosomes of *C. tepidum* in buffer solution (black) and transmission spectra of band-pass filters at 532 nm (green) and 740 nm (red). (c–f) Microscopic images of the same area of the sample taken in fluorescence (c), transmission at 740 nm (d) and 532 nm (f), and transmission difference at 740 nm (e). Scale bar in (f) corresponds to 500 nm. (g) Fluorescence intensity modulation as a function of the polarization of the excitation light at 733 nm (bottom of y-axis is set to 0). (h) Modulation of the transmitted intensity difference as a function of the polarization of the incident light at 740 nm (bottom of y-axis is set to 0).

the mutant chlorosomes exhibit a significantly lower degree of the inner structural disorder and much larger values of the angle of the exciton dipole moment with respect to the long axis.

2. MATERIALS AND METHODS

2.1. Sample Preparation. Cells of WT *C. tepidum* were grown at a light intensity of $\sim 100 \mu\text{mol photons m}^{-2} \text{ s}^{-1}$, and chlorosomes were isolated as described before.^{23,24} The pigment analysis was done using HPLC chromatography. The four main C8 and C12 homologues of BChl-*c* esterified with farnesyl at C17³ were combined together, including 3¹-R and 3¹-S epimers of each homologue. 8-Ethyl-12-ethyl BChl-*c* and 8-propyl-12-ethyl-BChl-*c* were the two most abundant homologues, accounting for 60% and 30% of the total content, respectively. The chlorosomes were stored in the dark in a freezer as concentrated suspensions in 50 mM Tris-HCl buffer, pH 8.0. Growth, isolation, and characterization of the chlorosomes of the *bchQ bchR bchU* triple mutant have been described elsewhere.^{15,22}

Samples for Microscopic Measurements. A small aliquot ($\sim 10 \mu\text{L}$) of the chlorosome suspension was thawed immediately before the experiment; for WT chlorosomes, the chlorosome suspension was diluted in 5 mL of Tris-HCl buffer (pH 8.0, 50 mM) or for triple mutant

it was diluted in 5 mL of PBS buffer (pH 7.4, 10 mM Na-phosphate, 150 mM NaCl), mixed with 10 mM Na₂S₂O₄. The diluted solution (50 μ L) was dropped onto a cleaned glass coverslip and left standing for 3–5 min to allow adsorption of the chlorosomes onto the substrate. The remaining solution was then washed away with a clean buffer. A thin (100 nm) layer of poly(vinyl alcohol) (PVA) was spin-coated on top of the chlorosomes from filtered 2 wt % PVA buffer solution to protect the chlorosomes from rapid oxidation. The samples were immediately used for experiments. Control experiments were also performed on dry samples without the PVA layer and on samples in a buffer solution.

To verify that we are measuring individual isolated chlorosomes, we also prepared samples of several different concentrations and counted the numbers of fluorescence spots in microscopic images of each sample. The numbers scaled proportionally with BChl_c concentration. In addition, we measured AFM images of samples prepared by the same method and with the same concentration as the samples for single-chlorosome optical microscopy, and we observed no effects of aggregation. We thus conclude that with very high probability the individual spots observed in optical microscopic images correspond to single isolated chlorosomes.

Samples for Bulk LD Measurements. Chlorosomes were diluted in a Tris-HCl buffer solution of 10% (w/v) acrylamide for appropriate optical density in a 10 mm optical cell. The solution was polymerized to obtain a polyacrylamide gel block with dimensions of 10 mm \times 10 mm \times 30 mm. Chlorosomes were oriented by an equal squeezing of the gel block along two perpendicular axes with a desired degree of compression n . The compression factor n was calculated as a ratio between the original and final dimension in one of the compression directions. The orientation process itself had no effect on the absorption spectrum of the chlorosomes.

2.2. Experimental Setup and Methods. *Microscopic LD Measurement and Analysis in Absorption and Fluorescence.* Microscopic linear dichroism measurements on single chlorosomes were carried out using an inverted fluorescence microscope Olympus IX71. The setup is shown schematically in Supporting Information (SI) in Figure S1. Absorption of single chlorosomes was detected using light from a tungsten lamp which passes either a 740 nm band-pass filter (corresponding to the absorption maximum of WT chlorosomes) or a 720 nm band-pass filter (corresponding to the absorption maximum of the mutant chlorosomes). The light further traveled through a manually rotated linear polarizer and was collimated onto the sample. Light transmitted through the sample was collected by an oil-immersion lens (Olympus UPlanFLN100xO2, N.A. 1.3) and detected with an electron-multiplying CCD camera (Andor iXon+). A series of CCD microscopic images was taken as a function of the angle of the linear polarization ψ of the incident light with respect to a reference. A control experiment was performed in the same manner with a 532 nm band-pass filter (corresponding to a minimal absorption of chlorosomes) to check that the observed decrease in the transmitted light was not caused by impurities in the sample or by refraction by the chlorosome.

Fluorescence of single chlorosomes was excited using a 733 nm cw diode laser (Pico Quant), which was spectrally filtered and circularly polarized with a quarter-wave plate. A rotating linear polarizer created slowly rotating excitation light that was linearly polarized in the sample plane at an angle ψ with respect to a reference. Fluorescence was collected by the same oil-immersion lens (Olympus UPlanFLN100xO2, N.A. 1.3) and detected with the electron-multiplying CCD camera after passing a dichroic mirror and a long-pass filter. A series of CCD microscopic images was taken as a function of the angle of the linear polarization ψ .

In a typical experiment, the chlorosomes were first identified in a fluorescence image. The laser was then blocked, the dichroic and long-pass filters were removed, and the transmission polarization modulation measurement at 740 nm (or 720 nm) and a control measurement at

532 nm were carried out. The laser was then unblocked, the filters were replaced, and the fluorescence polarization modulation experiment was performed. This sequence ensured that the most damaging experiment (long-time excitation of fluorescence) was done last. The effect of photodegradation is discussed in the SI. Typical fluorescence and transmission images are shown in SI as Figure S2. Fluorescence images were analyzed by integrating the CCD count from the whole diffraction-limited spot of each chlorosome and plotting the integrated count as fluorescence intensity I_F against the angle ψ . Transmission data were analyzed by fitting the cropped images of diffraction-limited spots of individual chlorosomes with 2D Gaussian functions. The average I_0 base level (100% transmission) was carefully determined for each chlorosome individually by examining its vicinity to avoid any distortion of the data. The peak of the Gaussian fit was then taken as the peak transmission value I_T , and the difference $\Delta I_T = I_0 - I_T$ was plotted against the angle ψ . The polarization modulated I_F and ΔI_T were both fit with a \cos^2 function, and the fit gave the values of $I_{F_{\min}}$ and $I_{F_{\max}}$ and $\Delta I_{T_{\min}}$ and $\Delta I_{T_{\max}}$ for the calculation of the degree of modulation M_F and M_T .

Spectral Measurements and Analysis. Fluorescence spectra were measured using an imaging spectrograph (Bunkou Keiki CLP-50, 0.5 nm resolution) placed between the microscope and the CCD camera. A fluorescence image was first taken with the spectrograph slit open and with the grating replaced with a mirror. The microscope stage was then shifted to position a single chlorosome at the center of the slit, the slit was closed, and the mirror removed to disperse the fluorescence and record a spectrum as a 2D image on the CCD camera. The spectra were analyzed by fitting with a sum of Gaussian functions (3 or 4, depending on the complexity of the spectral shapes) and the spectra peak positions and widths (full-width at half-maxima, fwhm) were determined from the fits.

Three-Dimensional Fluorescence-Detected Microscopic LD. The 3D LD was measured on single chlorosomes using the same fluorescence microscope by monitoring the polarization-modulated fluorescence intensity that was alternately excited by epi-illumination and by total internal reflection. Details on the method can be found elsewhere.²⁵

Bulk LD Measurement and Analysis. Linear dichroism at room temperature was measured using a Jasco-715 spectropolarimeter. The LD parameter P , defined as $P = (A_{\perp} - A_{\parallel})/A$ (where A_{\parallel} is absorbance of light polarized along the compression axis and A_{\perp} of light polarized perpendicular to the compression axis), was measured as a function of the compression n , and the resulting $P(n)$ dependence was fitted according to ref 26 with the equation

$$P(n) = \frac{3}{2} \langle (3 \cos^2 \gamma - 1) \rangle \frac{4n^2 - 1}{5n^2 + 1}$$

The above equation was derived in ref 26 to describe the effect of gel compression on the LD spectra. The chlorosome is modeled by a rod, and the angle γ is the angle between the chlorosome average transition dipole and its long axis. An example of the bulk LD measurement is shown in SI in Figure S4.

3. RESULTS AND DISCUSSION

Single-molecule spectroscopy is a method that helps to reveal nanometer-scale properties and processes in condensed and soft matter, and this approach has found widespread use in recent years. So far, single molecules have been detected mainly by monitoring their fluorescence. Direct measurement of absorption from a molecule is prevented by the quantum noise of light, which overwhelms most light intensity changes due to absorption by a single molecule. The early sophisticated double-modulation absorption experiments succeeded only in qualitative spectroscopic information on a single molecule.²⁷ However, chlorosomes represent a special case because they contain a very

large number of pigment molecules within a structure whose size is smaller than the diffraction limit of light. An estimate based on BChl-*c* absorption cross section, the number of BChl-*c* molecules in a chlorosome, and the diffraction limit indicates that light with a wavelength corresponding to the absorption peak passing a single chlorosome should be attenuated 3–5% by absorption (see SI for details). This value is well above the experimental noise and makes the direct detection of absorption by chlorosomes feasible.

The absorption spectrum of a solution of chlorosomes of WT *C. tepidum* is shown in Figure 1b. The peaks at 458 and 741 nm correspond to the BChl Soret and Q_y bands, respectively. These values are typical for bacteria grown under the conditions used in this work. Excitation of a single chlorosome in the Q_y band produces a fluorescence intensity (I_F) microscopic image, as shown in Figure 1c. The corresponding transmission image of the same area with a 740 nm band-pass filter (Figure 1d) shows a decrease of about 5% of the transmitted light intensity I_T at the location of the chlorosome. The difference transmitted intensity ΔI_T image, calculated as $I_0 - I_T$ (I_0 being the basal (blank) intensity level determined as described in the Materials and Methods), is shown in Figure 1e; it reflects the amount of light absorbed by the chlorosome. The ΔI_T images were used for further analysis. As a control experiment, a transmission image with a 532 nm filter, corresponding to the low-absorbance region by chlorosome carotenoids, was taken for each chlorosome. Figure 1f shows that no intensity drop occurs at 532 nm, confirming that the changes observed in Figure 1, d and e, correspond to the detection of light absorption by a chlorosome.

Analyses of fluorescence and transmission images, taken as a function of the angle ψ of the linearly polarized light yields modulated I_F and ΔI_T traces, respectively, are shown in Figure 1, g and h. The ΔI_T trace is directly related to the LD of a single chlorosome at the peak of the Q_y band. As seen from the data in Figure 1, the I_F trace is very similar in both the phase and degree of the modulation. The traces were evaluated in terms of the degree of modulation M , which is defined as the ratio I_{\min}/I_{\max} (see Figure 1, g and h) for both I_F and ΔI_T . The values M_F and M_T were measured for statistical ensembles of single chlorosomes and plotted as histograms in Figure 2, a and b. Both M_F and M_T show wide distributions of values. For comparison, Figure 2a also includes the M_F values obtained by exciting the fluorescence in the Soret band at 458 nm. The mean of the distribution is shifted toward higher M_F values due to generally different orientations of the Soret and Q_y transition dipoles, but its width is similar to that of the Q_y -band-excited M_F . Correlation between the transmission and fluorescence distributions in the Q_y band is shown in Figure 2c, in which, for easier comparison with bulk LD data, the modulations M_F and M_T were converted to the apparent angles γ_F and γ_T between averaged transition dipoles and the direction of I_{\max} as $\gamma_F = \tan^{-1}((I_{F_{\min}}/I_{F_{\max}})^{1/2})$ and $\gamma_T = \tan^{-1}((\Delta I_{T_{\min}}/\Delta I_{T_{\max}})^{1/2})$. The quantities γ_F and γ_T characterize the distribution of the exciton transition dipole moments within the chlorosome. If all the transition dipoles were parallel, the angles would be zero. The other extreme is a homogeneous distribution of the transition dipoles in all directions, which would lead to γ_F and γ_T values of 45°. The data in Figure 2c show high correlation, with the correlation coefficient $\rho = 0.63$, between γ_T and γ_F .

The high correlation indicates a direct relationship between the fluorescence and transmission data and implies that monitoring the Q_y band absorption LD via the fluorescence signal

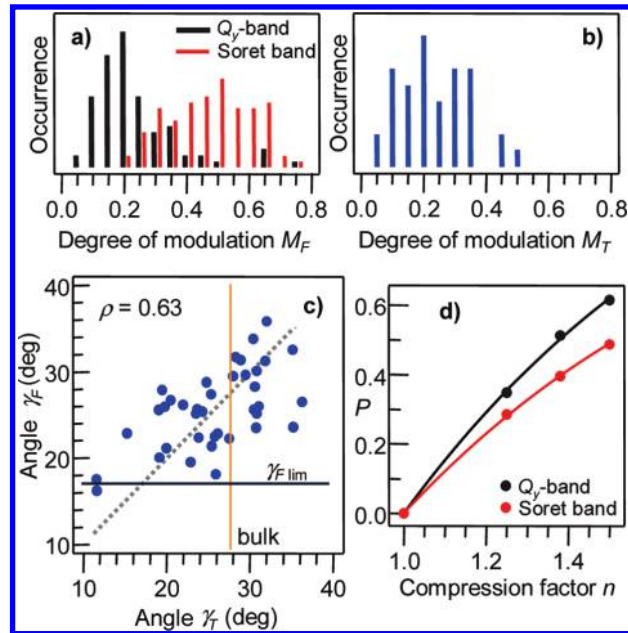


Figure 2. Linear dichroism measured on single chlorosomes of WT *C. tepidum*. (a) Histogram of the degree of modulation of fluorescence M_F excited in the Soret (red, 98 chlorosomes) and Q_y bands (black, 90 chlorosomes). (b) Histogram of the degree of modulation of the transmitted intensity difference M_T in the peak of the Q_y band (42 chlorosomes). (c) Correlation between the transmission and fluorescence distributions in the Q_y band plotted as the angles γ_F , γ_T . Yellow vertical line shows the bulk value γ obtained from fitting the data in (d). The horizontal line shows the limiting value of the angle γ_F . (d) Absorption anisotropy P measured as a function of the compression factor n of the polyacrylamide gel for the Soret (red) and Q_y bands (black).

does not distort the information due to potential differences in the fluorescence quantum yield along different axes of the chlorosome. We note that this is not an obvious result. Fluorescence anisotropy from single chlorosomes excited in the Soret band²⁸ also provided distribution of the fluorescence depolarization ratio (defined as $DP = (F_{\max} - F_{\min})/(F_{\max} + F_{\min})$), but the mean of the distribution was ~ 0.3 , compared to the absorption DP value of ~ 0.5 that would correspond to the mean of the distribution in Figure 2b. The difference can be attributed to uncorrelated relaxations from the Soret absorption levels to the Q_y -band emitting levels.

Mean values of the distributions are 25.8° for γ_T and 25.7° for γ_F . Generally, mean values of single-molecule distributions correspond to the average values obtained by measuring bulk samples. In bulk absorption LD experiments chlorosomes are usually oriented in compressed polyacrylamide gels, in which the chlorosome long axis is perpendicular to the compression axis.²⁶ Results of measurements on WT *C. tepidum* of the parameter P (see the Materials and Methods section for definition) as a function of the compression factor n at the peak wavelengths of the Soret and Q_y bands are shown in Figure 2d. Fitting of the data using the expression of ref 26 provided the averaged bulk angle γ , that is, the averaged orientation of the Q_y transition dipole moments with respect to the long axis of the chlorosome. The resulting value of 27.9° was in good agreement with the mean values of the two single-chlorosome distributions. For the Soret band the bulk value of γ was 34.0° which again agrees well with

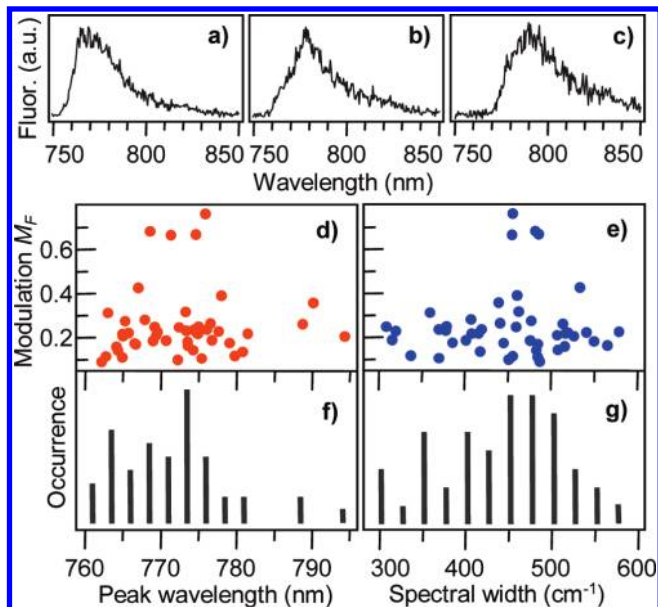


Figure 3. Spectroscopic characterization of single chlorosomes of WT *C. tepidum*. (a–c) Fluorescence spectra of three different chlorosomes at room temperature excited in the Q_y band at 733 nm. (d) Correlation between the degree of modulation M_F and the spectral peak wavelength. (e) Correlation between the degree of modulation M_F and the spectral width. (f) Histogram of the spectral peak wavelengths (47 chlorosomes). (g) Histogram of the spectral widths as full-widths at half-maxima (47 chlorosomes).

the mean value of 34.9° obtained from the Soret band γ_F distribution. Another result of the bulk LD measurement is that the direction of I_{\max} is coincident with the long axis of the chlorosome. As a chlorosome is smaller than the diffraction limit of light, it is not possible on the single-chlorosome level to relate the orientation of I_{\max} directly to the orientation of the chlorosome. Thus, the results of the bulk LD experiment provided an important feedback to the single-chlorosome experiments, and enabled the interpretation of the apparent angles γ_F , γ_T as the angles between averaged exciton transition dipole moments and the long axis of the chlorosome.

The large scatter of the γ_T and γ_F distributions is due to the presence of various kinds of disorder. Apart from the mean values, the small-angle cutoff values of the distributions provide additional important information; specifically, they provide a limit on the exciton dipole moment orientation angle that must be taken into account in molecular-level models of BChl organization. Since experimentally it is much easier to obtain reliable data from the fluorescence experiments, we determined the limiting value of the angle from the distribution in Figure 2a, which contained 90 chlorosomes. Averaging over the lowest 5% of the angles from the distribution, i.e., over the values corresponding to the lowest amount of disorder, we obtain $\gamma_{F\lim} = 17^\circ$. We will discuss implications of this value later.

As summarized in Figure 3, information on the nature of the disorder can be obtained from fluorescence spectra of single chlorosomes. Examples of spectra from three different chlorosomes in Figure 3, a, b, and c, show that there are large differences in positions of spectral peaks and in spectral widths of fluorescence from BChl-*c* molecules associated with individual chlorosomes. Fluorescence from BChl-*a* was not detected, probably because the experimental conditions used were not sufficient to

achieve fully anoxic conditions and the BChl-*a* fluorescence was partly quenched. Moreover, it has been shown that even under fully anoxic conditions, adsorption of the chlorosome to a solid substrate leads to disappearance of fluorescence from BChl-*a*.²⁹ The spectra of an ensemble of 47 chlorosomes were analyzed by fitting with a sum of Gaussian functions, and the results are plotted in histograms in Figure 3, f and g.

The histograms show large distributions of both spectral peaks and spectral widths (fwhm), similar to those observed before.³⁰ The means of the histograms are 773 nm for the peaks and 446 cm^{-1} for the widths, in good agreement with bulk spectral data.³¹ Generally, both the spectral peak and spectral width are determined by the excitonic properties of the aggregates. Distributions of these parameters imply the presence of excitonic disorder. Both diagonal and off-diagonal disorder, as well as the distribution of exciton coherent lengths, would cause distributions of the spectral peaks and widths. In order to look into the origin of the disorder observed in the LD parameters, correlations between the degree of modulation M_F and the spectral parameter distributions were plotted (Figure 3, d, e). It is obvious that there was no correlation between M_F and either spectral peak or spectral width in single chlorosomes, that is, no correlation was observed between the disorder measured in the absorption LD and the excitonic disorder. This observation indicated that the disorder measured in the LD was primarily due to the mesoscopic inner structural disorder of the chlorosomes and that the excitonic disorder that was also present did not manifest itself in the LD parameter distributions.

In the following discussion, we try to relate the observations made on single chlorosomes of WT *C. tepidum* with a simplified model of the supramolecular structure of BChls in chlorosomes. Earlier cryo-EM studies and, especially the recently published end-on cryo-EM images,¹⁴ indicate that the BChl suprastructure of chlorosomes is formed by 2D-aggregates that are curved to a varying extent to form curved lamellae, arcs and helical scrolls, or are completely enclosed in the form of concentric cylinder-like structures. These types of arrangements are schematically shown in Figure 4a. We note that the arrangement in Figure 4a is meant to only schematically sketch the main structural motifs, not to reproduce details of the structure deduced from NMR and cryo-EM studies. The 2D-aggregates are curved or rolled along the long (*z*) axis of the chlorosome. In either case, we may model the arrangement by a primary structural unit of a quarter-cylinder (Figure 4b). The arrows in Figure 4b indicate orientations of the aggregate transition dipole moments, not orientations of individual BChl-*c* molecules. Depending on the delocalization length, the orientation of the exciton transition can be different from the orientation of the monomer stacks. We assume that the quarter-cylinder is large enough to contain many delocalized excitons. From the symmetry of the structures, it is obvious that in the absence of any structural disorder along the *z*-axis the projection γ_F onto the sample plane of the sum of the exciton transition dipoles of the chlorosome and that of the quarter-cylinder would be same. Assuming that the exciton transition dipoles on the quarter-cylinder are all oriented in the same direction with respect to its surface, such orientation of the dipoles gives a unique value of the projection angle γ_F . As shown in Figure 4c, the orientation of the exciton dipole is characterized by two angles defined with respect to the *z*-axis: an in-plane angle ϕ_i (in the *x*–*z*-plane of the aggregate) and an out-of-plane angle ϕ_o (in the *y*–*z*-plane perpendicular to the aggregate). We may now use the limiting values of γ_F from the distribution in Figure 2c (which

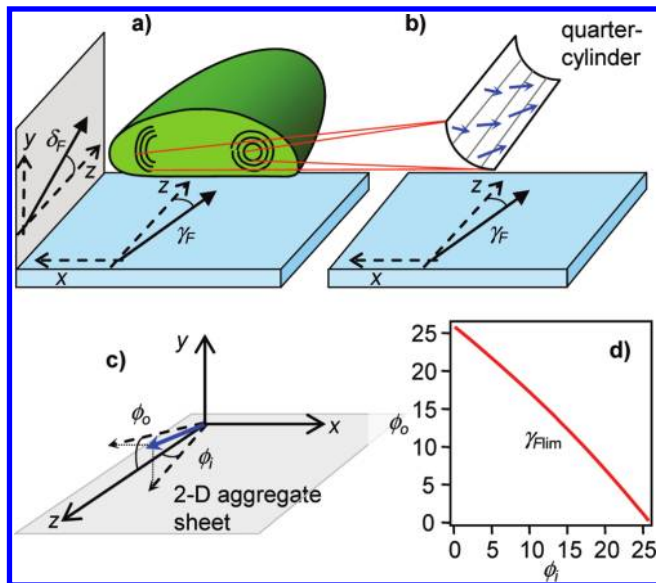


Figure 4. (a) Schematic structure of a chlorosome and measured angles of the projected transition dipole moment with respect to long axis z in the $x-z$ -plane (γ_F) and in the $y-z$ -plane (δ_F). (b) Model of the primary structural unit as a 2D-aggregate quarter-cylinder, and projection of the sum of the 2D-aggregate exciton transition dipole moments onto the sample plane. (c) Orientation of the exciton transition dipole moment with respect to the aggregate surface. (d) Range of possible values of the angles ϕ_i and ϕ_o of the exciton transition dipoles obtained from the limiting value $\gamma_{F \text{ lim}}$ for WT *C. tepidum*.

are related to chlorosomes with the least amount of structural disorder) and estimate the values of ϕ_i and ϕ_o that would give the corresponding projection angle $\gamma_{F \text{ lim}}$. This can be done by a simple geometrical consideration, which is described in detail in the SI. The result is shown in Figure 4d. It can be seen that, for the limiting cases of zero in-plane or zero out-of-plane angles, the remaining angles are approximately 25° . Between these two extremes the graph describes the possible combinations of ϕ_i and ϕ_o that correspond to the value of $\gamma_{F \text{ lim}}$ of 17° . It should be noted that the line in the Figure 4d should be considered an upper limit for the angles ϕ_i and ϕ_o because the $\gamma_{F \text{ lim}}$ value is not necessarily free of any effects of disorder, both structural and excitonic. The limiting in-plane angle ϕ_i can now be compared to the orientation of the BChl monomer Q_y transition dipoles in the plane of the 2D-aggregate as obtained from the NMR and cryo-EM study of *C. tepidum*.¹⁵ The value of 25° measured here is smaller than the value of approximately 35° , which can be deduced from Figure 5C of ref 15. However, it should be stressed that our measurement provides the angle of the exciton transition dipole moment of the aggregate, and this is generally different from the monomer dipole angle due to the delocalization (coherent length) of the exciton.³²

By measuring the LD parameters in all three spatial dimensions, the question of the symmetry in the excitonic properties and its relationship to the symmetry of the inner structure of chlorosomes can be tested. Structures rotationally symmetric along the z -axis would give the same value of LD parameters when viewed from top ($x-z$ -plane) and from side ($y-z$ -plane). We have recently reported a microscopic method that allows one to measure fluorescence detected 3D LD of nanoparticles with subwavelength dimensions.²⁵ Application of this method to individual chlorosomes provided the projection angle γ_F of

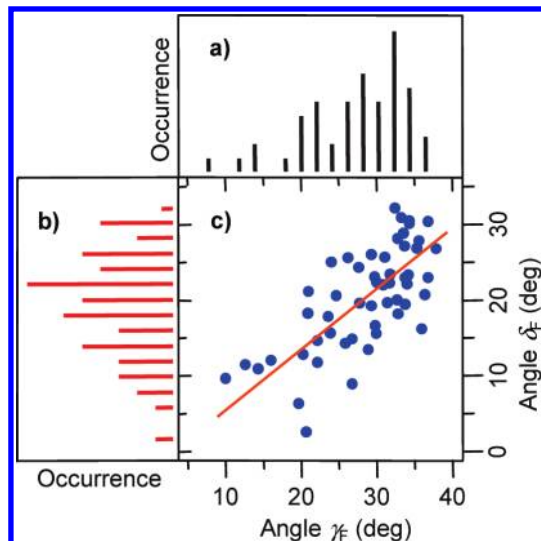


Figure 5. Three-dimensional linear dichroism of single chlorosomes of WT *C. tepidum*. (a) Histogram of the angle γ_F of the transition dipole of single chlorosomes in the $x-z$ -plane (53 chlorosomes). (b) Histogram of the angle δ_F of the transition dipole of single chlorosomes in the $y-z$ -plane (53 chlorosomes). (c) Correlation between the angles γ_F and δ_F . The line represents a linear fit.

the transition dipole in the $x-z$ -plane and at the same time the projection angle δ_F of the transition dipole in the $y-z$ -plane (Figure 4a). It should be stressed that the relationship of δ_F to the chlorosome geometry was obtained directly, and it was not necessary to compare it with results obtained for chlorosomes in compressed gels. It is reasonable to expect that most of the chlorosomes were oriented in parallel to the substrate. The parallel orientation was verified by measuring AFM images of chlorosomes adsorbed from solution on a microscope slide glass (see Supporting Information). Therefore, the orientation of the chlorosome with respect to the $y-z$ -plane is well-defined in this microscopic experiment. Moreover, there is a considerable possibility that the chlorosomes are attached to the cover glass by the baseplate; this would not change the parallel orientation and thus would have no effect on the interpretation of the data. The experimental results for WT *C. tepidum* are shown in Figure 5. Histogram of the angle γ_F (Figure 5a) is similar to that in Figure 2 and provides an identical value of the limit $\gamma_{F \text{ lim}}$ of 17° . The histogram of the angle δ_F is similar in shape but its mean is shifted to 20.3° and the limiting value $\delta_{F \text{ lim}}$ for this angle (calculated from the same data points as $\gamma_{F \text{ lim}}$) is 10° . The correlation between δ_F and γ_F shown in Figure 5c provides a relationship between the two angles in the form of $\delta_F/\gamma_F = 0.72$.

The overall shift to lower angles in the $y-z$ -plane and the $\delta_F/\gamma_F = 0.72$ relationship reflect the lack of symmetry of the inner structure of the chlorosomes, as reported also by the end-on cryo-EM images of WT *C. tepidum*.¹⁴ The inner structure (as seen in Figure 1 bottom, from ref 14) is a combination of curved lamellae, open arcs, scrolls, and completely enclosed cylinders. The open structures tend to be oriented along the longer axis (x -axis) of the chlorosome cross section. Projections of transition dipole moments of these 2D-aggregates onto the $x-z$ - and $y-z$ -planes thus provide different values of the angles γ_F and δ_F . These different values together with symmetric angles from the cylindrical structures then combine to give the observed asymmetry in the $x-z$ - and $y-z$ -planes. Even though the published

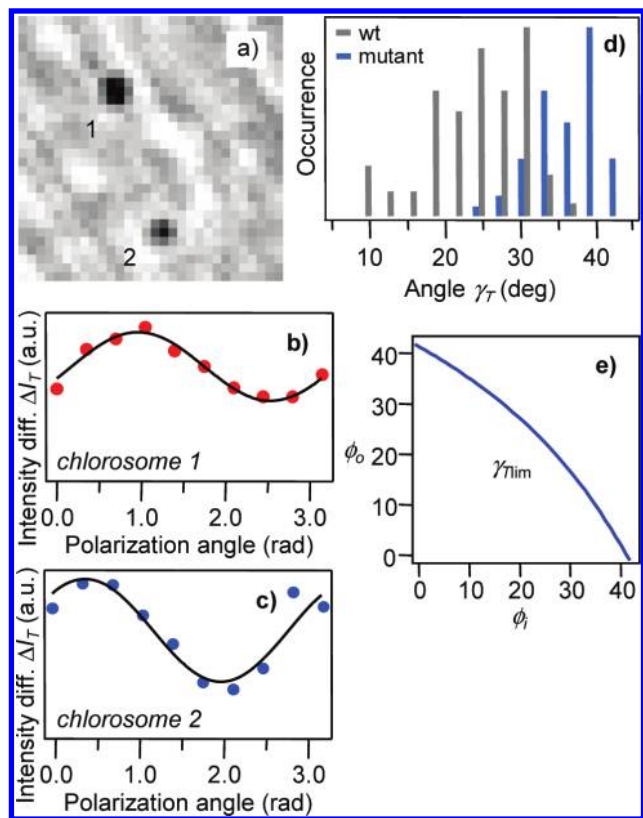


Figure 6. Absorption linear dichroism measured on single chlorosomes of the *bchQ bchR bchU* triple mutant *C. tepidum*. (a) Transmission microscopic image of at the Q_y peak of the absorption spectrum. The dark spots 1 and 2 correspond to decrease of transmission due to absorption of single chlorosomes. (b, c) Examples of polarization-modulated transmission traces obtained from chlorosomes 1 and 2 in the image in a). (d) Histogram of the angle γ_T of the absorption transition dipole of single chlorosomes in the x - z -plane; blue = triple mutant (54 chlorosomes), gray = wild type (42 chlorosomes). (e) Range of possible values of the angles ϕ_i and ϕ_o of the exciton transition dipoles obtained from the limiting value γ_T^{lim} .

cryo-EM images¹⁴ do not allow for a quantitative comparison of the inner suprastructure with the asymmetry observed by the 3D LD, there is a good qualitative agreement between the two methods. This is despite the markedly different experimental conditions—chlorosomes embedded in amorphous ice at cryogenic temperatures¹⁴ and polymer-coated, surface-adsorbed chlorosomes at room-temperature (this work). The 3D LD thus offers a promising alternative for the study of other photosynthetic antenna complexes.

It is now instructive to compare the LD results obtained on WT *C. tepidum* with chlorosomes which are known to have a very well-ordered suprastructure. Chlorosomes from the *bchQ bchR bchU* triple mutant *C. tepidum* are composed mainly of 2D-aggregates that are completely enclosed into large concentric cylinders (Figure 4 of ref 15). Within the aggregates, individual BChl molecules are oriented with their Q_y transition dipole moments at 55° with respect to the cylinder long axis.¹⁵ Results on the triple mutant single-chlorosome absorption LD are summarized in Figure 6.

An example of a transmission microscopic image at the Q_y peak of the mutant absorption spectrum (720 nm) is shown in Figure 6a. The two dark spots correspond to two isolated

chlorosomes. The polarization-modulated ΔI_T traces obtained from the two chlorosomes are presented in Figure 6, b and c. The modulation depth of the two traces is somewhat different, pointing to the presence of a certain amount of disorder even in the mutant chlorosomes. The disorder has been quantified by plotting a histogram of the absorption LD parameter γ_T for Figure 6d (blue bars). It is evident from the figure that there is still a distribution of the γ_T angle. However, when compared to the results for WT chlorosomes (gray bars), the distribution is much narrower, indicating a significantly lower degree of inner structural disorder. The remaining disorder can be understood in the context of the top-view cryo-EM images,¹⁵ which show that the cylinders are not always completely parallel along the length of the chlorosome. Slightly different distributions of orientations along the z -axis in different chlorosomes would result in a distribution of the LD parameters such as the γ_T angle. We also cannot rule out some distortion of the chlorosomes that might occur as a result of their adsorption on the glass surface. Other important differences compared to the WT chlorosomes are the mean and the lower limiting values of the angle γ_T . The mean γ_T is 37.3° (compared to 25.8° for the WT), while the limiting γ_T^{lim} is 30° (compared to 17° for the WT). These differences are compatible with the different molecular level organization of the BChls in WT and *bchQ bchR bchU* mutant chlorosomes as reported before,¹⁵ that is, with the fact that BChl *syn-anti* monomer stacks that form the 2D sheets are oriented perpendicular to the chlorosome long axis in the mutant and parallel to it in the WT. This structural difference is nicely corroborated in the LD results reported here.

We further use the quarter-cylinder model introduced above for the WT chlorosomes and calculate the range of allowed angles ϕ_i and ϕ_o of the exciton transition dipole moments with respect to the surface of the 2D sheet. Even though the main structural component in the *bchQ bchR bchU* triple mutant chlorosomes is a complete cylinder, for the purpose of reconstructing the exciton dipole orientation the quarter-cylinder gives the same results. Moreover, the cylinders are wrapped in loosely bound sheets, and these sheets are better described by the quarter-cylinder model. The results are shown in Figure 6e. For the limiting cases of zero ϕ_i or zero ϕ_o angles, the remaining angles are approximately 42° (compared to 25° for the WT chlorosomes). Similarly to the WT, the value of 42° is smaller than the 55° estimated for the orientation of the BChl monomer Q_y transition dipoles with respect to the cylinder long axis.¹⁵ The structural model for the *bchQ bchR bchU* triple mutant¹⁵ is a helical cylinder that consists of a stack of BChl rings, each of them slightly rotated with respect to the previous one. It has been shown theoretically³³ that excitons in such cylindrical aggregate contain a component polarized along the cylinder long axis ($k_2 = 0$) and degenerate components polarized perpendicular to it ($k_2 = \pm 1$). The ratio of the parallel and perpendicular components gives rise to the observed angle of the excitonic transition. This angle is generally different from the angle of the BChl-*c* monomer dipoles and depends on the length of the cylinder.^{32,33} Finally, results on the 3D LD for the mutant chlorosomes (data shown as Figure S8 in SI) provide a relation $\delta_F/\gamma_F = 0.93$. This value indicates much higher symmetry of the inner structural organization of the mutant chlorosomes due to the presence of well-ordered symmetric cylinders as the prevailing structural unit.

We note that the discussion on structural disorder and its effect on the excitonic properties refer to static disorder. Apart from the static disorder there are also dynamic processes that lead

to a spatial redistribution of the exciton density in a cylindrical aggregate. It has been shown by simulations³² that this relaxation takes place on the order of ~ 100 fs, that is, much faster than the time scale of the present experiments.

In conclusion, we characterized the absorption anisotropy of single chlorosomes of both wild-type and triple mutant of the photosynthetic bacterium *C. tepidum* by measuring directly the absorption LD and three-dimensional fluorescence-detected LD on individual chlorosomes. The results revealed large structural disorder along the chlorosome long axis in the WT and negligible correlation with excitonic energy disorder. Importantly, the results indicate that the usual ensemble (bulk) LD experiments reported so far in literature have been influenced by the effect of the mesoscopic structural disorder and have provided incorrect values of the transition dipole moment orientations. Consistent with the structural data,¹⁵ chlorosomes from the triple mutant show a significantly lower amount of the inner disorder and different angles of the orientation of the exciton transition dipoles with respect to the chlorosome long axis. The exciton orientation angles are important parameters that have to be taken into account in any future models of the excitonic properties of chlorosomes.

■ ASSOCIATED CONTENT

S Supporting Information. Estimation of light intensity decrease by transmission of a single chlorosome. Illustrations of the experimental setup, correspondence between fluorescence and transmission images, examples of polarization modulated absorption of single WT chlorosomes, effect of photodegradation and evolution of bulk LD spectra at increasing gel compression. Estimation of the possible orientation of exciton transition dipole from the observed angle γ_F lim. AFM microscopy of single adsorbed chlorosomes. General remarks on the relationship between bulk and single-chlorosome experiments and 3D LD on mutant chlorosomes. Complete ref 8. This material is available free of charge via the Internet at <http://pubs.acs.org>.

■ AUTHOR INFORMATION

Corresponding Author

vacha.m.aa@m.titech.ac.jp

■ ACKNOWLEDGMENT

We would like to thank Prof. Jakub Psencik from the Charles University in Prague for extended and invaluable discussions and for many critical comments. The work was supported by the Grant-in-Aid for Scientific Research 20340109 of the Japan Society for the Promotion of Science (M.V.), the Global Center of Excellence program in materials science (M.V., S.H.), and the Czech Science Foundation Project 206/09/0375 (F.V.).

■ REFERENCES

- Blankenship, R. E.; Matsuura, K. In *Light-Harvesting Antennas*; Green, B. R., Parson, W. W., Eds.; Kluwer Academic Publishers: Dordrecht, 2003; pp 195–217.
- Frigaard, N. U.; Bryant, D. A. In *Microbiology Monographs*; Shivley, J. M., Ed.; Springer: Berlin, Heidelberg, 2006; Vol. 2, pp 79–114.
- Bryant, D. A.; Garcia Costas, A. M.; Maresca, J. A.; Gomez Maqueo Chew, A.; Klatt, C. G.; Bateson, M. M.; Tallon, L. J.; Hostetler, J.; Nelson, W. C.; Heidelberg, J. F.; Ward, D. M. *Science* **2007**, *317*, 523–526.
- Montano, G. A.; Bowen, B. P.; LaBelle, J. T.; Woodbury, N. W.; Pizziconi, V. B.; Blankenship, R. E. *Biophys. J.* **2003**, *85*, 2560–2565.
- Balaban, T. S.; Tamiaki, H.; Holzwarth, A. R. *Top. Curr. Chem.* **2005**, *258*, 1–38.
- Beatty, J. T.; Overmann, J.; Lince, M. T.; Manske, A. K.; Lang, A. S.; Blankenship, R. E.; Van Dover, C. L.; Martinson, T. A.; Plumley, F. G. *Proc. Natl. Acad. Sci. U.S.A.* **2005**, *102*, 9306–9310.
- Overmann, J.; Cypionka, H.; Pfennig, N. *Limnol. Oceanogr.* **1992**, *37*, 150–155.
- Balaban, T. S.; *Chem.—Eur. J.* **2005**, *11*, 2267–2275.
- Staehelin, L. A.; Golecki, J. R.; Fuller, R. C.; Drews, G. *Arch. Microbiol.* **1978**, *119*, 269–277.
- Staehelin, L. A.; Golecki, J. R.; Drews, G. *Biochim. Biophys. Acta* **1980**, *589*, 30–45.
- Psencik, J.; Ikonen, T. P.; Laurinmaki, P.; Merckel, M. C.; Butcher, S. J.; Serimaa, R. E.; Tuma, R. *Biophys. J.* **2004**, *87*, 1165–1172.
- Psencik, J.; Arellano, J. B.; Ikonen, T. P.; Borrego, C. M.; Laurinmaki, P. A.; Butcher, S. J.; Serimaa, R. E.; Tuma, R. *Biophys. J.* **2006**, *91*, 1433–1440.
- Psencik, J.; Collins, A. M.; Liljeroos, L.; Torkkeli, M.; Laurinmaki, P.; Ansink, H. M.; Ikonen, T. P.; Serimaa, R. E.; Blankenship, R. E.; Tuma, R.; Butcher, S. J. *J. Bacteriol.* **2009**, *191*, 6701–6708.
- Oostergetel, G. T.; Reus, M.; Gomez Maqueo Chew, A.; Bryant, D. A.; Boekema, E. J.; Holzwarth, A. R. *FEBS Lett.* **2007**, *581*, 5435–5439.
- Ganapathy, S.; Oostergetel, G. T.; Wawrzyniak, P. K.; Reus, M.; Gomez Maqueo Chew, A.; Buda, F.; Boekema, E. J.; Bryant, D. A.; Holzwarth, A. R.; de Groot, H. J. M. *Proc. Natl. Acad. Sci. U.S.A.* **2009**, *106*, 8525–8530.
- Nozawa, T.; Ohtomo, K.; Suzuki, M.; Nakagawa, H.; Shikama, Y.; Konami, H.; Wang, Z. Y. *Photosynth. Res.* **1994**, *41*, 211–223.
- Holzwarth, A. R.; Schaffner, K. *Photosynth. Res.* **1994**, *41*, 225–233.
- Egawa, A.; Fujiwara, T.; Mizoguchi, T.; Kakitani, Y.; Koyama, Y.; Akutsu, H. *Proc. Natl. Acad. Sci. U.S.A.* **2007**, *104*, 790–795.
- Jochum, T.; Malla Reddy, C.; Eichhofer, A.; Butth, G.; Szmytkowski, J.; Kalt, H.; Moss, D.; Balaban, T. S. *Proc. Natl. Acad. Sci. U.S.A.* **2008**, *105*, 12736–12741.
- Van Rossum, B. J.; Steensgaard, D. B.; Mulder, F. M.; Boender, G. J.; Schaffner, K.; Holzwarth, A. R.; de Groot, H. J. M. *Biochemistry* **2001**, *40*, 1587–1595.
- Saga, Y.; Shibata, Y.; Tamiaki, H. *J. Photochem. Photobiol. C* **2010**, *11*, 15–24.
- Gomez Maqueo Chew, A.; Frigaard, N. U.; Bryant, D. A. *J. Bacteriol.* **2007**, *189*, 6176–6184.
- Steengaard, D. B.; Matsuura, K.; Cox, R. P.; Miller, M. *Photochem. Photobiol.* **1997**, *65*, 129–134.
- Arellano, J. B.; Borrego, C. M.; Martinez-Planells, A.; Garcia-Gil, L. J. *Arch. Microbiol.* **2001**, *175*, 226–233.
- Furumaki, S.; Habuchi, S.; Vacha, M. *Chem. Phys. Lett.* **2010**, *487*, 312–314.
- Van Amerongen, H.; Vasmel, H.; Van Grondelle, R. *Biophys. J.* **1988**, *54*, 65–76.
- Moerner, W. E.; Kador, L. *Phys. Rev. Lett.* **1989**, *62*, 2535–2538.
- Shibata, Y.; Saga, Y.; Tamiaki, H.; Itoh, S. *Photosynth. Res.* **2009**, *100*, 67–78.
- Shibata, Y.; Saga, Y.; Tamiaki, H.; Itoh, S. *Biophys. J.* **2006**, *91*, 3787–3796.
- Saga, Y.; Wazawa, T.; Mizoguchi, T.; Ishii, Y.; Yanagida, T.; Tamiaki, H. *Photochem. Photobiol.* **2002**, *75*, 433–436.
- Hohmann-Marriott, M. F.; Blankenship, R. E. *Biochim. Biophys. Acta* **2007**, *1767*, 106–113.
- Prokhorenko, V. I.; Steensgaard, D. B.; Holzwarth, A. R. *Biophys. J.* **2003**, *85*, 3173–3186.
- Didraga, C.; Klugkist, J. A.; Knoester, J. *J. Phys. Chem. B* **2002**, *106*, 11474–11486.